Journal of Sound and Vibration (1999) **224**(5), 879–895
Article No. jsvi.1999.2202, available online at http://www.idealibrary.com on IDEAL®

INVERSE DYNAMICS CONTROL OF CONSTRAINED ROBOTS IN THE PRESENCE OF JOINT FLEXIBILITY

S. KEMAL IDER

Mechanical Engineering Department, Middle East Technical University, Ankara 06531, *Turkey*

(*Received* 2 *June* 1998, *and in final form* 8 *February* 1999)

An inverse dynamics control algorithm for constrained flexible-joint robots is developed. It is shown that in a flexible-joint robot, the acceleration level inverse dynamic equations are singular because of the elastic media. Implicit numerical integration methods that account for the higher order derivative information are utilized for solving the singular set of differential equations. The control law proposed linearizes and decouples the system and achieves simultaneous and asymptotically stable trajectory tracking control of the end-effector motion and contact forces. Together with the integrators for improving robustness due to modelling errors and disturbances, a fifth order position error dynamics and a third order contact force error dynamics are obtained. A 3R spatial robot with all joints flexible is simulated to illustrate the performance of the method.

1. INTRODUCTION

In many applications of industrial robots such as assembling, scraping, grinding and deburring, the end-effector contacts a surface and the control of contact forces and torques in certain directions of the task space is necessary. To successfully accomplish such constrained maneouvres the contact forces and the motion along the constraint surfaces should be controlled simultaneously.

The hybrid force and position control schemes based on rigid models are limited in their applicability due to the flexibilities in the robot structure. It has been experimentally shown that for a variety of robots, joint flexibility is the principal source contributing to overall robot flexibility [1]. Sources of joint flexibility include harmonic drives, couplings, belt drives and shafts. As the joint flexibility can cause instability of robot control, especially for force-controlled robots, it should be included in the controller design [2].

Among the motion control methods for flexible-joint robots, an inverse dynamics approach yields linear subsystems for each degree of freedom [3–6]. A singular perturbation approach considers a reduced order model by decomposing the system into slow and fast subsystems [7, 8]. Adaptive control strategies have also been developed based on reduced order models to compensate for parametric and dynamic uncertainties [9, 10].

0022-460X/99/300879 + 17 $30.00/0

Only a few studies have dealt with the hybrid force and motion control problem of flexible-joint robots. Jankowski and Elmaraghy [11] presented an analytical inverse dynamics control scheme. Here the input–output relation is found analytically by eliminating the intermediate variables. This elimination requires the differentiation of the equations of motion and the acceleration level constraint and task equations twice. The resulting complexity of the control law yields this approach unsuitable for real-time implementation especially for robots with three or more joints. Hu and Goldenberg [12] developed a procedure for the hybrid motion and force control of co-ordinated robot arms in the presence of joint flexibility. The model order is reduced by decomposing the system into two subsystems. First, motion and force controllers are designed to generate the desired joint elastic force. Then a joint elastic force controller is used to regulate the joint elastic force. However, this approach is limited in applicability since it is based on the assumption that the joint springs are sufficiently stiff so that the flexible joint dynamics is much faster than the manipulator dynamics.

The aim of this study is to develop a control law for hybrid force and motion trajectory tracking control of flexible-joint robots which avoids the drawbacks of the existing algorithms. It is shown that the inverse dynamic equations of the system form a singular set of differential equations. This is because the control forces cannot affect the task accelerations and contact forces instantaneously due to the elastic media, resulting in the inverse dynamic problem being time anticipatory [13]. The higher order derivative information is taken into account by utilizing methods for solving singular sets of differential equations, thus avoiding further differentiation of the dynamic equations. The control law developed achieves simultaneous and asymptotically stable end-effector position and contact force control by feedback of joint positions, joint velocities and rotor velocities. The desired motion and force trajectories are allowed to involve initial and intermediate discontinuities in all their states. For illustration, a 3R spatial robot subject to discontinuous motion and force trajectories is simulated in the presence of modelling error.

2. DYNAMIC MODEL

A flexible joint robot is modelled as n links and n actuator rotors connected by elastic transmissions with speed reduction. It is assumed that the rotor mass distribution about its axis of rotation is symmetric, and the rotational kinetic energy of the rotor is mainly due to its own rotation [3, 11, 12]. Let θ_i, $i = 1, \ldots, n$, denote the joint co-ordinates and ψ_i, $i = 1, \ldots, n$, the rotor angles divided by the gear ratio r_i. The system has $2n$ degrees of freedom while only n control actuator torques T_i, $i = 1, \ldots, n$, are available. The elasticity of the transmission at the ith joint is modelled as a torsional spring with stiffness k_i. Structural damping which is inherent in structural members used in drive trains is considered as a structural damping coefficient d_i, $i = 1, \ldots, n$. With the assumptions stated above, the inertia and gravitational coupling terms between the joint and rotor variables disappear yielding the following dynamic equations:

$$\mathbf{M}(\boldsymbol{\theta})\ddot{\boldsymbol{\theta}} + \mathbf{Q}(\boldsymbol{\theta}, \dot{\boldsymbol{\theta}}) + \mathbf{D}(\dot{\boldsymbol{\theta}} - \dot{\boldsymbol{\psi}}) + \mathbf{K}(\boldsymbol{\theta} - \boldsymbol{\psi}) + \mathbf{F}^{\mathrm{c}} = \mathbf{0}, \tag{1}$$

$$\mathbf{I}^{\mathrm{r}}\ddot{\boldsymbol{\psi}} + \mathbf{D}^{\mathrm{r}}\dot{\boldsymbol{\psi}} - \mathbf{D}(\dot{\boldsymbol{\theta}} - \dot{\boldsymbol{\psi}}) - \mathbf{K}(\boldsymbol{\theta} - \boldsymbol{\psi}) = \mathbf{T}, \tag{2}$$

where $\mathbf{M}(\boldsymbol{\theta})$ is the symmetric positive-definite inertia matrix corresponding to the joint degrees of freedom, $\mathbf{Q}(\boldsymbol{\theta}, \dot{\boldsymbol{\theta}})$ is the vector of centrifugal, Coriolis and gravitational forces, $\mathbf{F}^c$ is the vector of generalized contact forces, $\mathbf{K} = \text{diag}[k_i]$, $\mathbf{D} = \text{diag}[d_i]$, $\mathbf{I}^r = \text{diag}[r_i^2 I_i^r]$, where I_i^r is the moment of inertia of the ith rotor about its rotation axis, and $\mathbf{D}^r = \text{diag}[r_i^2 D_i^r]$, where D_i^r is the viscous damping coefficient of the ith rotor. $\mathbf{M}$ and $\mathbf{Q}$ are same as those for the n-link rigid robot where the rotor masses (as point masses) are included as part of the corresponding links.

The prescribed end-effector contact forces and the prescribed end-effector trajectories along the constraint surfaces represent the tasks of the manipulator. Let the dimension of the task space be n, and let x_i, $i = 1, \ldots, n$, denote the Cartesian end-effector position and orientation co-ordinates which can be expressed as $\mathbf{x} = \boldsymbol{\phi}(\boldsymbol{\theta})$. The joint and task space velocity relation is $\dot{\mathbf{x}} = \mathbf{J}(\boldsymbol{\theta})\dot{\boldsymbol{\theta}}$, where $\mathbf{J}$ is the manipulator Jacobian matrix. It is assumed that the singular positions are out of the operation range so that $\mathbf{J}$ never becomes singular.

The contact of the end-effector with the environment can be described by constraint equations

$$g_i(\mathbf{x}, t) = 0, \quad i = 1, \ldots, m. \tag{3a}$$

Differentiating equation (3a) and writing $\mathbf{x}$ and $\dot{\mathbf{x}}$ in terms of $\boldsymbol{\theta}$ and $\dot{\boldsymbol{\theta}}$, the following velocity relation is obtained:

$$E_{ij}(\boldsymbol{\theta}, t)\dot{\boldsymbol{\theta}}_j + G_i(\boldsymbol{\theta}, t) = 0, \quad i = 1, \ldots, m. \tag{3b}$$

The generalized contact forces are

$$\mathbf{F}^c = \mathbf{E}^T\boldsymbol{\lambda}, \tag{4}$$

where $\boldsymbol{\lambda}$ is the vector of Lagrange multipliers that represent the contact forces and moments, which are perpendicular to the constraint surfaces.

Let y_i, $i = 1, \ldots, n - m$ represent the independent co-ordinates of the end-effector along the constraint surfaces, which can be expressed as

$$y_i = h_i(\mathbf{x}, t). \tag{5a}$$

This leads to the following velocity relation:

$$\dot{y}_i = P_{ij}(\boldsymbol{\theta}, t)\dot{\boldsymbol{\theta}}_j + H_i(\boldsymbol{\theta}, t), \quad i = 1, \ldots, n - m. \tag{5b}$$

Using equations (3b) and (5b), and denoting

$$\begin{bmatrix} \mathbf{E} \\ \mathbf{P} \end{bmatrix}^{-1} = [\boldsymbol{\eta} \ \boldsymbol{\mu}],$$

where $n \times m$ matrix $\boldsymbol{\eta}$ and the $n \times (n - m)$ matrix $\boldsymbol{\mu}$ are functions of positions only, $\dot{\boldsymbol{\theta}}$ is expressed in terms of $\dot{\mathbf{y}}$ as

$$\dot{\boldsymbol{\theta}} = \boldsymbol{\mu}\dot{\mathbf{y}} - (\boldsymbol{\eta}\mathbf{G} + \boldsymbol{\mu}\mathbf{H}). \tag{6}$$

When the intermediate variables $\boldsymbol{\psi}$ and $\boldsymbol{\theta}$ are eliminated in the dynamic equations, the relation between the input $\mathbf{T}$ and the outputs $\mathbf{y}$ and $\boldsymbol{\lambda}$ can be obtained as

$$(\mathbf{I}^{\mathrm{r}}\mathbf{K}^{-1}\mathbf{M}\boldsymbol{\mu})\overset{(4)}{\mathbf{y}} + (\mathbf{I}^{\mathrm{r}}\mathbf{K}^{-1}\mathbf{E}^{\mathrm{T}})\ddot{\boldsymbol{\lambda}} + \mathbf{A}(\ddot{\mathbf{y}}, \ddot{\mathbf{y}}, \dot{\mathbf{y}} \cdot \mathbf{y} \cdot \dot{\boldsymbol{\lambda}}, \boldsymbol{\lambda}) = \mathbf{T} + (\mathbf{K}^{-1}\mathbf{D})\dot{\mathbf{T}}, \tag{7}$$

where

$$\begin{aligned}\mathbf{A} = \mathbf{K}^{-1}\{\mathbf{I}^{\mathrm{r}}[\mathbf{M}(3\dot{\boldsymbol{\mu}}\ddot{\mathbf{y}} + 3\ddot{\boldsymbol{\mu}}\dot{\mathbf{y}} + \dddot{\boldsymbol{\mu}}\mathbf{y} - (\dddot{\boldsymbol{\eta}}\mathbf{G} + 3\ddot{\boldsymbol{\eta}}\dot{\mathbf{G}} + 3\dot{\boldsymbol{\eta}}\ddot{\mathbf{G}} + \boldsymbol{\eta}\dddot{\mathbf{G}} + \ddot{\boldsymbol{\mu}}\mathbf{H} + 3\dot{\boldsymbol{\mu}}\dot{\mathbf{H}} + 3\dot{\boldsymbol{\mu}}\ddot{\mathbf{H}} \\ + \boldsymbol{\mu}\dddot{\mathbf{H}}) + 2\dot{\mathbf{M}}\ddot{\boldsymbol{\theta}} + \ddot{\mathbf{M}}\dot{\boldsymbol{\theta}} + \ddot{\mathbf{Q}} + \mathbf{D}\ddot{\boldsymbol{\theta}} + \mathbf{K}\dot{\boldsymbol{\theta}} + \ddot{\mathbf{E}}^{\mathrm{T}}\boldsymbol{\lambda} + 2\dot{\mathbf{E}}^{\mathrm{T}}\dot{\boldsymbol{\lambda}})] + \mathbf{D}^{\mathrm{r}}(\mathbf{D}\ddot{\boldsymbol{\theta}} + \mathbf{K}\dot{\boldsymbol{\theta}}) \\ + (\mathbf{D} + \mathbf{D}^{\mathrm{r}})(\mathbf{M}\ddot{\boldsymbol{\theta}} + \dot{\mathbf{M}}\dot{\boldsymbol{\theta}} + \dot{\mathbf{Q}} + \dot{\mathbf{E}}^{\mathrm{T}}\boldsymbol{\lambda} + \mathbf{E}^{\mathrm{T}}\dot{\boldsymbol{\lambda}})\} + \mathbf{M}\ddot{\boldsymbol{\theta}} + \mathbf{Q} + \mathbf{E}^{\mathrm{T}}\boldsymbol{\lambda}\end{aligned} \tag{8}$$

and $\boldsymbol{\theta}$, $\dot{\boldsymbol{\theta}}$, $\ddot{\boldsymbol{\theta}}$ and $\dddot{\boldsymbol{\theta}}$ can be written in terms of $\mathbf{y}$, $\dot{\mathbf{y}}$, $\ddot{\mathbf{y}}$ and $\dddot{\mathbf{y}}$ using equation (6), its derivatives, and equations (3a) and (5a). An inverse dynamics control law can be formulated using equation (7). Specifying $\overset{(4)}{\mathbf{y}}$ and $\dddot{\boldsymbol{\lambda}}$ according to their desired values and the errors in their states, one can calculate $\mathbf{T} + (\mathbf{K}^{-1}\mathbf{D})\dot{\mathbf{T}}$ from equation (7), and numerical integration can be used for finding the corresponding control torque vector $\mathbf{T}$. However, this requires $\dot{\mathbf{M}}$, $\ddot{\mathbf{M}}$, $\dot{\mathbf{Q}}$, $\ddot{\mathbf{Q}}$, and the second and third derivatives of $\boldsymbol{\mu}$, $\boldsymbol{\eta}$, $\mathbf{G}$ and $\mathbf{H}$. The resulting expressions become extremely long and complex especially for $n \geqslant 3$, yielding this approach impractical for real-time applications.

3. INVERSE DYNAMICS CONTROL USING SINGULAR ACCELERATION LEVEL EQUATIONS

To formulate an inverse dynamics control law, the dynamic equations will be utilized at the acceleration level to find the input torques required to achieve the desired end-effector motion and contact forces. To this end, equations (1) and (2) and the time derivatives of equations (3b) and (5b) can be written in augmented from as shown below, where $\ddot{\mathbf{y}}$ and $\boldsymbol{\lambda}$ are replaced by control variables $\mathbf{z}$ and $\boldsymbol{\Gamma}$ that represent "command accelerations" and "command contact forces", respectively,

$$\begin{bmatrix} \mathbf{M} & \mathbf{0} & \mathbf{0} \\ \mathbf{0} & \mathbf{I}^{\mathrm{r}} & -\mathbf{I} \\ \mathbf{E} & \mathbf{0} & \mathbf{0} \\ \mathbf{P} & \mathbf{0} & \mathbf{0} \end{bmatrix} \begin{bmatrix} \ddot{\boldsymbol{\theta}} \\ \ddot{\boldsymbol{\psi}} \\ \mathbf{T} \end{bmatrix} = \begin{bmatrix} -\mathbf{Q} - \mathbf{D}(\dot{\boldsymbol{\theta}} - \dot{\boldsymbol{\psi}}) - \mathbf{K}(\boldsymbol{\theta} - \boldsymbol{\psi}) - \mathbf{E}^{\mathrm{T}}\boldsymbol{\Gamma} \\ -\mathbf{D}^{\mathrm{r}}\dot{\boldsymbol{\psi}} + \mathbf{D}(\dot{\boldsymbol{\theta}} - \dot{\boldsymbol{\psi}}) + \mathbf{K}(\boldsymbol{\theta} - \boldsymbol{\psi}) \\ -\dot{\mathbf{E}}\dot{\boldsymbol{\theta}} - \dot{\mathbf{G}} \\ -\dot{\mathbf{P}}\dot{\boldsymbol{\theta}} - \dot{\mathbf{H}} + \mathbf{z} \end{bmatrix}. \tag{9}$$

It is seen from equation (7) that, in the forward dynamics, a torque vector $\mathbf{T}$ instantaneously affects the end-effector jerk rate $\overset{(4)}{\mathbf{y}}$ and the contact force second

derivative $\ddot{\boldsymbol{\lambda}}$. Hence, in the control law the "command jerk rates" $\ddot{\mathbf{z}}$ and the "command contact force second derivatives" $\ddot{\boldsymbol{\Gamma}}$ need to be specified. Using the desired jerk rates, the desired contact force second derivatives, and the errors in the end-effector motion and force states, $\ddot{\mathbf{z}}$ and $\ddot{\boldsymbol{\Gamma}}$ can be formulated as

$$\ddot{\mathbf{z}} = \overset{(4)^{\mathrm{d}}}{\mathbf{y}} + \mathbf{C}_1(\dddot{\mathbf{y}}^{\mathrm{d}} - \dddot{\mathbf{y}}) + \mathbf{C}_2(\ddot{\mathbf{y}}^{\mathrm{d}} - \ddot{\mathbf{y}}) + \mathbf{C}_3(\dot{\mathbf{y}}^{\mathrm{d}} - \dot{\mathbf{y}}) + \mathbf{C}_4(\mathbf{y}^{\mathrm{d}} - \mathbf{y}) + \mathbf{C}_5 \int (\mathbf{y}^{\mathrm{d}} - \mathbf{y})\, \mathrm{d}t \tag{10}$$

and

$$\ddot{\boldsymbol{\Gamma}} = \ddot{\boldsymbol{\lambda}}^{\mathrm{d}} + \mathbf{B}_1(\dot{\boldsymbol{\lambda}}^{\mathrm{d}} - \dot{\boldsymbol{\lambda}}) + \mathbf{B}_2(\boldsymbol{\lambda}^{\mathrm{d}} - \boldsymbol{\lambda}) + \mathbf{B}_3 \int (\boldsymbol{\lambda}^{\mathrm{d}} - \boldsymbol{\lambda})\, \mathrm{d}t, \tag{11}$$

where superscript d denotes desired values, and $\mathbf{C}_i$, $i = 1, \ldots, 5$ and $\mathbf{B}_i$, $i = 1, 2, 3$ are constant feedback gain diagonal matrices, i.e., $\mathbf{C}_i = \mathrm{diag}\,[C_{ij}]$, $j = 1, \ldots, n - m$ and $\mathbf{B}_i = \mathrm{diag}\,[B_{ij}]$, $j = 1, \ldots, m$. The integral terms in equations (10) and (11) are included for improving robustness to model errors and disturbances.

To show that the application of the control torque vector $\mathbf{T}$ as obtained from the solution of equation (9) linearizes the decouples the system, consider the fact that, in the absence of modelling error and disturbances, the actual accelerations and contact forces produced by the control torques are equal to $\mathbf{z}$ and $\boldsymbol{\Gamma}$, respectively, i.e., $\ddot{\mathbf{y}} = \mathbf{z}$ and $\boldsymbol{\lambda} = \boldsymbol{\Gamma}$. Using equations (10) and (11), this leads to the following error dynamics:

$$\overset{(4)}{\mathbf{e}}_{\mathrm{p}} + \mathbf{C}_1 \dddot{\mathbf{e}}_{\mathrm{p}} + \mathbf{C}_2 \ddot{\mathbf{e}}_{\mathrm{p}} + \mathbf{C}_3 \dot{\mathbf{e}}_{\mathrm{p}} + \mathbf{C}_4 \mathbf{e}_{\mathrm{p}} + \mathbf{C}_5 \int \mathbf{e}_{\mathrm{p}}\, \mathrm{d}t = 0 \tag{12}$$

and

$$\ddot{\mathbf{e}}_{\mathrm{f}} + \mathbf{B}_1 \dot{\mathbf{e}}_{\mathrm{f}} + \mathbf{B}_2 \mathbf{e}_{\mathrm{f}} + \mathbf{B}_3 \int \mathbf{e}_{\mathrm{f}}\, \mathrm{d}t = 0, \tag{13}$$

where $\mathbf{e}_{\mathrm{p}} = \mathbf{y}^{\mathrm{d}} - \mathbf{y}$ and $\mathbf{e}_{\mathrm{f}} = \boldsymbol{\lambda}^{\mathrm{d}} - \boldsymbol{\lambda}$. Asymptotic stability is achieved by appropriate choice of the feedback gains C_{ij} and B_{ij}. Norms such as ITAE, IAE, etc. can be used for this purpose.

However, the solution of equation (9) for the control torque vector $\mathbf{T}$ is not a straightforward task, since the acceleration and torque coefficient matrix is singular.

In fact, in the inverse dynamics problem, the first, third and fourth rows of equation (9) involve only the kinematic variables, and will be termed as the inverse kinematic equations. On the other hand, the second row of equation (9) is used for

finding the corresponding control torques. The inverse kinematic equations can be expressed as

$$\begin{bmatrix} \mathbf{M} & \mathbf{0} \\ \mathbf{E} & \mathbf{0} \\ \mathbf{P} & \mathbf{0} \end{bmatrix} \begin{bmatrix} \ddot{\boldsymbol{\theta}} \\ \ddot{\boldsymbol{\psi}} \end{bmatrix} = \begin{bmatrix} -\mathbf{Q} - \mathbf{D}(\dot{\boldsymbol{\theta}} - \dot{\boldsymbol{\psi}}) - \mathbf{K}(\boldsymbol{\theta} - \boldsymbol{\psi}) - \mathbf{E}^{\mathrm{T}}\boldsymbol{\Gamma} \\ -\dot{\mathbf{E}}\dot{\boldsymbol{\theta}} - \dot{\mathbf{G}} \\ -\dot{\mathbf{P}}\dot{\boldsymbol{\theta}} - \dot{\mathbf{H}} + \mathbf{z} \end{bmatrix}. \tag{14}$$

However, equation (14) cannot be solved in this form because it represents a singular set of differential equations. The physical reason for the singularity is that, because the control torques are transmitted to the end-effector through the elastic joints, the control torques do not have an instantaneous effect on the end-effector accelerations and contact forces. This means that the inverse dynamics problem is time-anticipatory.

Since the acceleration coefficient matrix in equation (14) cannot be inverted to obtain an explicit system of ordinary differential equations, implicit numerical integration methods need to be used [14]. Here the backward Euler method will be utilized. This is the simplest implicit integration method where the numerical integration is based on the following backward difference formula:

$$\dot{\mathbf{s}}_{k+1} = \frac{1}{h}(\mathbf{s}_{k+1} - \mathbf{s}_k), \tag{15}$$

where h is the sampling time interval and k is the time step number. Using equation (15), equation (9) can be written at time t_{k+1} as

$$\mathbf{M}\tfrac{1}{h}(\dot{\boldsymbol{\theta}}_{k+1} - \dot{\boldsymbol{\theta}}_k) + \mathbf{Q} + \mathbf{D}(\dot{\boldsymbol{\theta}}_{k+1} - \dot{\boldsymbol{\psi}}_{k+1}) + \mathbf{K}(h\dot{\boldsymbol{\theta}}_{k+1} + \boldsymbol{\theta}_k - \mathbf{h}\dot{\boldsymbol{\psi}}_{k+1} - \boldsymbol{\psi}_k) + \mathbf{E}^{\mathrm{T}}\boldsymbol{\Gamma}_{k+1} = 0, \tag{16}$$

$$\mathbf{I}^{\mathrm{r}}\tfrac{1}{h}(\dot{\boldsymbol{\psi}}_{k+1} - \dot{\boldsymbol{\psi}}_k) + \mathbf{D}^{\mathrm{r}}\dot{\boldsymbol{\psi}}_{k+1} - \mathbf{D}(\dot{\boldsymbol{\theta}}_{k+1} - \dot{\boldsymbol{\psi}}_{k+1}) - \mathbf{K}(h\dot{\boldsymbol{\theta}}_{k+1} + \boldsymbol{\theta}_k - h\dot{\boldsymbol{\psi}}_{k+1} - \boldsymbol{\psi}_k) = \mathbf{T}_{k+1}, \tag{17}$$

$$\mathbf{E}\tfrac{1}{h}(\dot{\boldsymbol{\theta}}_{k+1} - \dot{\boldsymbol{\theta}}_k) + \dot{\mathbf{E}}\dot{\boldsymbol{\theta}}_{k+1} + \dot{\mathbf{G}} = 0, \tag{18}$$

$$\mathbf{P}\tfrac{1}{h}(\dot{\boldsymbol{\theta}}_{k+1} - \dot{\boldsymbol{\theta}}_k) + \dot{\mathbf{P}}\dot{\theta}_{k+1} + \dot{\mathbf{H}} = \mathbf{z}_{k+1}, \tag{19}$$

where $\mathbf{M}(h\dot{\boldsymbol{\theta}}_{k+1} + \boldsymbol{\theta}_k)$, $\mathbf{Q}(h\dot{\boldsymbol{\theta}}_{k+1} + \boldsymbol{\theta}_k, \dot{\boldsymbol{\theta}}_{k+1})$, $\mathbf{E}(h\dot{\boldsymbol{\theta}}_{k+1} + \boldsymbol{\theta}_k, t)$, $\dot{\mathbf{E}}(h\dot{\boldsymbol{\theta}}_{k+1} + \boldsymbol{\theta}_k, \dot{\boldsymbol{\theta}}_{k+1}, t)$, $\mathbf{P}(h\dot{\boldsymbol{\theta}}_{k+1} + \boldsymbol{\theta}_k, t)$, $\dot{\mathbf{P}}(h\dot{\boldsymbol{\theta}}_{k+1} + \boldsymbol{\theta}_k, \dot{\boldsymbol{\theta}}_{k+1}, t)$, $\dot{\mathbf{G}}(h\dot{\boldsymbol{\theta}}_{k+1} + \boldsymbol{\theta}_k, \dot{\boldsymbol{\theta}}_{k+1}, t)$ and $\dot{\mathbf{H}}(h\dot{\boldsymbol{\theta}}_{k+1} + \boldsymbol{\theta}_k, \dot{\boldsymbol{\theta}}_{k+1}, t)$, also depend on $\dot{\boldsymbol{\theta}}_{k+1}$. Equations (16)–(19) represent a set of $3n$ algebraic equations from which the $3n$ unknowns $\dot{\boldsymbol{\theta}}_{k+1}$, $\dot{\boldsymbol{\psi}}_{k+1}$ and $\mathbf{T}_{k+1}$ can be solved, as described below.

At this point it is necessary to determine the command contact forces $\boldsymbol{\Gamma}_{k+1}$ and the command accelerations $\mathbf{z}_{k+1}$. Usually, the desired motion and force trajectories are specified as piecewise smooth functions. Let $\mathbf{y}^{\mathrm{d}}(t)$ be smooth up to the third

derivative in the time interval $t_a \leqslant t < t_b$. Then integration of equation (10) twice at this interval leads to

$$\begin{aligned}\mathbf{z} = \mathbf{z}_a + \dot{\mathbf{z}}_a(t-t_a) + \ddot{\mathbf{y}}^{\mathrm{d}} - \ddot{\mathbf{y}}_a^{\mathrm{d}} - \dddot{\mathbf{y}}_a^{\mathrm{d}}(t-t_a) + \mathbf{C}_1[(\dot{\mathbf{y}}^{\mathrm{d}} - \dot{\mathbf{y}}) - (\dot{\mathbf{y}}_a^{\mathrm{d}} - \dot{\mathbf{y}}_a) \\ - (\ddot{\mathbf{y}}_a^{\mathrm{d}} - \ddot{\mathbf{y}}_a)(t-t_a)] + \mathbf{C}_2[(\mathbf{y}^{\mathrm{d}} - \mathbf{y}) - (\mathbf{y}_a^{\mathrm{d}} - \mathbf{y}_a) - (\dot{\mathbf{y}}_a^{\mathrm{d}} - \dot{\mathbf{y}}_a)(t-t_a)] \\ - \mathbf{C}_3(\mathbf{y}_a^{\mathrm{d}} - \mathbf{y}_a)(t-t_a) + \mathbf{C}_3\int_{t_a}^{t}\dddot{\mathbf{w}}(\tau)\,\mathrm{d}\tau + \mathbf{C}_4\int_{t_a}^{t}\left[\int_{t_a}^{\tau}\dddot{\mathbf{w}}(s)\,\mathrm{d}s\right]\mathrm{d}\tau \\ + \mathbf{C}_5\int_{t_a}^{t}\left\{\int_{t_a}^{\tau}\left[\int_{t_a}^{s}\dddot{\mathbf{w}}(u)\,\mathrm{d}u\right]\mathrm{d}s\right\}\mathrm{d}\tau, \qquad t_a \leqslant t < t_b, \end{aligned} \tag{20}$$

where $\dddot{\mathbf{w}} = \mathbf{y}^{\mathrm{d}} - \mathbf{y}$. Evaluation of equation (20) at time t_{k+1}, where for $\mathbf{y}$, $\mathbf{y}^{\mathrm{d}}$ and their derivatives the values at time t_k are used because of discretization, yields $\mathbf{z}_{k+1}$ as

$$\begin{aligned}\mathbf{z}_{k+1} = \mathbf{z}_a + \dot{\mathbf{z}}_a(t_{k+1}-t_a) + \ddot{\mathbf{y}}_k^{\mathrm{d}} - \ddot{\mathbf{y}}_a^{\mathrm{d}} - \dddot{\mathbf{y}}_a^{\mathrm{d}}(t_{k+1}-t_a) + \mathbf{C}_1[(\dot{\mathbf{y}}_k^{\mathrm{d}} - \dot{\mathbf{y}}_k) - (\dot{\mathbf{y}}_a^{\mathrm{d}} - \dot{\mathbf{y}}_a) \\ - (\ddot{\mathbf{y}}_a^{\mathrm{d}} - \ddot{\mathbf{y}}_a)(t_{k+1}-t_a)] + \mathbf{C}_2[(\mathbf{y}_k^{\mathrm{d}} - \mathbf{y}_k) - (\mathbf{y}_a^{\mathrm{d}} - \mathbf{y}_a) - (\dot{\mathbf{y}}_a^{\mathrm{d}} - \dot{\mathbf{y}}_a)(t_{k+1}-t_a)] \\ - \mathbf{C}_3(\mathbf{y}_a^{\mathrm{d}} - \mathbf{y}_a)(t_{k+1}-t_a) + \mathbf{C}_3(h\ddot{\mathbf{w}}_{k+1} + \ddot{\mathbf{w}}_k) + \mathbf{C}_4(h^2\ddot{\mathbf{w}}_{k+1} + h\ddot{\mathbf{w}}_k + \dot{\mathbf{w}}_k) \\ + \mathbf{C}_5(h^3\dddot{\mathbf{w}}_{k+1} + h^2\ddot{\mathbf{w}}_k + h\dot{\mathbf{w}}_k + \mathbf{w}_k), \quad t_a \leqslant t_k < t_b, \end{aligned} \tag{21}$$

where $\dddot{\mathbf{w}}_{k+1} = \mathbf{y}_k^{\mathrm{d}} - y_k$.

Integration of equation (11) twice in the interval $t_a \leqslant t < t_b$ yields

$$\begin{aligned}\boldsymbol{\Gamma} = \boldsymbol{\Gamma}_a + \dot{\boldsymbol{\Gamma}}_a(t-t_a) + \boldsymbol{\lambda}^{\mathrm{d}} - \boldsymbol{\lambda}_a^{\mathrm{d}} - \dot{\boldsymbol{\lambda}}_a^{\mathrm{d}}(t-t_a) - \mathbf{B}_1(\boldsymbol{\lambda}_a^{\mathrm{d}} - \boldsymbol{\lambda}_a)(t-t_a) \\ + \mathbf{B}_1\int_{t_a}^{t}\ddot{\mathbf{p}}(\tau)\,\mathrm{d}\tau + \mathbf{B}_2\int_{t_a}^{t}\left[\int_{t_a}^{\tau}\ddot{\mathbf{p}}(s)\,\mathrm{d}s\right]\mathrm{d}\tau + \mathbf{B}_3\int_{t_a}^{t}\left\{\int_{t_a}^{\tau}\left[\int_{t_a}^{s}\ddot{\mathbf{p}}(u)\,\mathrm{d}u\right]\mathrm{d}s\right\}\mathrm{d}\tau, \\ t_a \leqslant t < t_b, \end{aligned} \tag{22}$$

where $\ddot{\mathbf{p}} = \boldsymbol{\lambda}^{\mathrm{d}} - \boldsymbol{\lambda}$. Then $\boldsymbol{\Gamma}_{k+1}$ is similarly obtained as

$$\begin{aligned}\boldsymbol{\Gamma}_{k+1} = \boldsymbol{\Gamma}_a + \dot{\boldsymbol{\Gamma}}_a(t_{k+1}-t_a) + \boldsymbol{\lambda}_k^{\mathrm{d}} - \boldsymbol{\lambda}_a^{\mathrm{d}} - \dot{\boldsymbol{\lambda}}_a^{\mathrm{d}}(t_{k+1}-t_a) - \mathbf{B}_1(\boldsymbol{\lambda}_a^{\mathrm{d}} - \boldsymbol{\lambda}_a)(t_{k+1}-t_a) \\ + \mathbf{B}_1(h\ddot{\mathbf{p}}_{k+1} + \ddot{\mathbf{p}}_k) + \mathbf{B}_2(h^2\ddot{\mathbf{p}}_{k+1} + h\ddot{\mathbf{p}}_k + \dot{\mathbf{p}}_k) \\ + \mathbf{B}_3(h^3\ddot{\mathbf{p}}_{k+1} + h^2\ddot{\mathbf{p}}_k + h\dot{\mathbf{p}}_k + \mathbf{p}_k), \end{aligned} \tag{23}$$

where $\ddot{\mathbf{p}}_{k+1} = \boldsymbol{\lambda}_k^d - \boldsymbol{\lambda}_k$.

It is important to note that, because the control torques cannot affect the end-effector accelerations, contact forces and their first time derivatives instantaneously, a step change in $\mathbf{z}$, $\dot{\mathbf{z}}$, $\boldsymbol{\Gamma}$ or $\dot{\boldsymbol{\Gamma}}$ require infinitely large control torques. This condition is avoided by choosing the integration constants such that $\mathbf{z}$, $\dot{\mathbf{z}}$, $\boldsymbol{\Gamma}$ or $\dot{\boldsymbol{\Gamma}}$ are matched at the discontinuities of the desired motions. This is achieved by setting $\mathbf{z}_a = \mathbf{z}(t_a^+) = \mathbf{z}(t_a^-)$, $\dot{\mathbf{z}}_a = \dot{\mathbf{z}}(t_a^+) = \dot{\mathbf{z}}(t_a^-)$, $\boldsymbol{\Gamma}_a = \boldsymbol{\Gamma}(t_a^+) = \boldsymbol{\Gamma}(t_a^-)$ and $\dot{\boldsymbol{\Gamma}}_a = \dot{\boldsymbol{\Gamma}}(t_a^+) = \dot{\boldsymbol{\Gamma}}(t_a^-)$.

In a singular set of differential equations (which are termed differential/algebraic equations in state variable representation) the initial conditions are not independent [14]. The relations that the initial conditions should satisfy can be found by using equation (14). To this end, the second and third rows of equation (14) are written as

$$\mathbf{R}\ddot{\boldsymbol{\theta}} = \mathbf{S}, \tag{24}$$

where

$$\mathbf{R} = \begin{bmatrix} \mathbf{E} \\ \mathbf{P} \end{bmatrix} \quad \text{and} \quad \mathbf{S} = \begin{bmatrix} -\dot{\mathbf{E}}\dot{\boldsymbol{\theta}} - \dot{\mathbf{G}} \\ -\dot{\mathbf{P}}\dot{\boldsymbol{\theta}} - \dot{\mathbf{H}} + \mathbf{z} \end{bmatrix}.$$

Premultiplying equation (24) by $\mathbf{MR}^{-1}$ and subtracting the resulting equation from the first row of equation (14), one obtains

$$\mathbf{MR}^{-1}\mathbf{S} + \mathbf{Q} + \mathbf{D}(\dot{\boldsymbol{\theta}} - \dot{\boldsymbol{\psi}}) + \mathbf{K}(\boldsymbol{\theta} - \boldsymbol{\psi}) + \mathbf{E}^{\mathrm{T}}\boldsymbol{\Gamma} = \mathbf{0}. \tag{25}$$

For the calculation of the control torques $\mathbf{T}_{k+1}$ from equations (16)–(19), the initial values $\boldsymbol{\theta}_k$, $\dot{\boldsymbol{\theta}}_k$, $\boldsymbol{\psi}_k$ and $\dot{\boldsymbol{\psi}}_k$ are needed. If $\boldsymbol{\theta}_k$, $\dot{\boldsymbol{\theta}}_k$, $\boldsymbol{\psi}_k$ and $\dot{\boldsymbol{\psi}}_k$ are measured at time t_k, then they will not satisfy equation (25) in the presence of modelling error and disturbance. This inconsistency causes the control torques $\mathbf{T}_{k+1}$ to be incorrect. In fact as $h \to 0$, they diverge. Either of the intermediate variables $\boldsymbol{\psi}_k$ or $\dot{\boldsymbol{\psi}}_k$ can be solved from equation (25) in order to achieve the consistency. Choosing $\boldsymbol{\psi}_k$ for this purpose, it can be calculated from equation (25) at time t_k as

$$\boldsymbol{\psi}_k = \boldsymbol{\theta}_k + \mathbf{K}^{-1}\lfloor \mathbf{MR}^{-1}\mathbf{S} + \mathbf{Q} + \mathbf{D}(\dot{\boldsymbol{\theta}}_k - \dot{\boldsymbol{\psi}}_k) + \mathbf{E}^{\mathrm{T}}\boldsymbol{\Gamma}_k \rfloor, \tag{26}$$

where $\boldsymbol{\theta}_k$, $\dot{\boldsymbol{\theta}}_k$ and $\dot{\boldsymbol{\psi}}_k$ are the measured quantities,

$$S = \begin{bmatrix} -\dot{\mathbf{E}}\dot{\boldsymbol{\theta}}_k - \dot{\mathbf{G}} \\ -\dot{\mathbf{P}}\dot{\boldsymbol{\theta}}_k - \dot{\mathbf{H}} + \mathbf{z}_k \end{bmatrix}$$

and $\mathbf{M}$, $\mathbf{Q}$, $\mathbf{E}$, $\mathbf{P}$, $\dot{\mathbf{E}}$, $\dot{\mathbf{G}}$, $\dot{\mathbf{P}}$ and $\dot{\mathbf{H}}$ are calculated using $\boldsymbol{\theta}_k$ and $\dot{\boldsymbol{\theta}}_k$.

The calculation of the control torques that linearize and decouple the system can be done in the following order.

Equations (18) and (19) represent n non-linear algebraic equations from which $\dot{\boldsymbol{\theta}}_{k+1}$ can be solved. $\mathbf{z}_{k+1}$ in equation (19) is given by equation (21) where $\mathbf{y}_k$ and $\dot{\mathbf{y}}_k$ are calculated from the measured $\boldsymbol{\theta}_k$ and $\dot{\boldsymbol{\theta}}_k$ using equations (5a, b).

Then equation (16) is used for finding $\dot{\boldsymbol{\psi}}_{k+1}$ as

$$\dot{\boldsymbol{\psi}}_{k+1} = (\mathbf{K}h + \mathbf{D})^{-1}\left[\mathbf{M}\tfrac{1}{h}(\dot{\boldsymbol{\theta}}_{k+1} - \dot{\boldsymbol{\theta}}_k) + \mathbf{Q} + \mathbf{E}^{\mathrm{T}}\boldsymbol{\Gamma}_{k+1} + \mathbf{K}(\boldsymbol{\theta}_k - \boldsymbol{\psi}_k)\right] + \dot{\boldsymbol{\theta}}_{k+1}, \tag{27}$$

where $\boldsymbol{\Gamma}_{k+1}$ is given by equation (23). The contact force vector $\boldsymbol{\lambda}_k$, that appears in equation (23), can be obtained by measurement. In general, feedback of the

measured force allows the local compensation for a mismatch between the modelled and the real systems. However, to avoid the difficulty of the contact force measurements, $\boldsymbol{\lambda}_k$ can be solved utilizing the constraint surface equation. To this end, substitution of $\ddot{\boldsymbol{\theta}}$ obtained from equation (1) into the derivative of equation (3b) at time t_k yields

$$\boldsymbol{\lambda}_k = -(\mathbf{E}\mathbf{M}^{-1}\mathbf{E}^{\mathrm{T}})^{-1}\{\mathbf{E}\mathbf{M}^{-1}[\mathbf{Q} + \mathbf{D}(\dot{\boldsymbol{\theta}}_k - \dot{\boldsymbol{\psi}}_k) + \mathbf{K}(\boldsymbol{\theta}_k - \boldsymbol{\psi}_k)] + \dot{\mathbf{E}}\dot{\boldsymbol{\theta}}_k + \dot{\mathbf{G}}\}, \quad (28)$$

where $\mathbf{M}$, $\mathbf{Q}$, $\mathbf{E}$, $\dot{\mathbf{E}}$, and $\dot{\mathbf{G}}$ are calculated using $\boldsymbol{\theta}_k$ and $\dot{\boldsymbol{\theta}}_k$.

Finally, the control torques $\mathbf{T}_{k+1}$ are computed from equation (17).

4. NUMERICAL EXAMPLE

The 3R spatial manipulator shown in Figure 1 represents one of the most common arm configurations used in industry. All three joints are assumed to be flexible. The weights act in the $-y$ direction. Initially, the system is at rest and the end point A is located at $x_{1_0} = 0{\cdot}3170\,\mathrm{m}$, $x_{2_0} = 0{\cdot}6160\,\mathrm{m}$ and $x_{3_0} = 0{\cdot}1830\,\mathrm{m}$ that corresponds to $\theta_1 = -30^\circ$, $\theta_2 = 120^\circ$ and $\theta_3 = -150^\circ$. Point A is required to exert a specified normal force profile composed of a cycloidal rise, constant level and a cycloidal return, on the plane surface $x = x_{1_0}$, while at the same time make a cycloidal deployment motion on that surface. The desired motion and force trajectories are given as

$$x_2^{\mathrm{d}} = \begin{cases} 0{\cdot}66\,\mathrm{m}, & 0 \leqslant t < T_1, \\ 0{\cdot}66 + \dfrac{0{\cdot}5}{T}\left[t - T_1 - \dfrac{T}{2\pi}\sin\dfrac{2\pi(t - T_1)}{T}\right]\mathrm{m}, & T_1 \leqslant t < T_1 + T, \\ 1{\cdot}16\,\mathrm{m}, & t \geqslant T_1 + T, \end{cases}$$

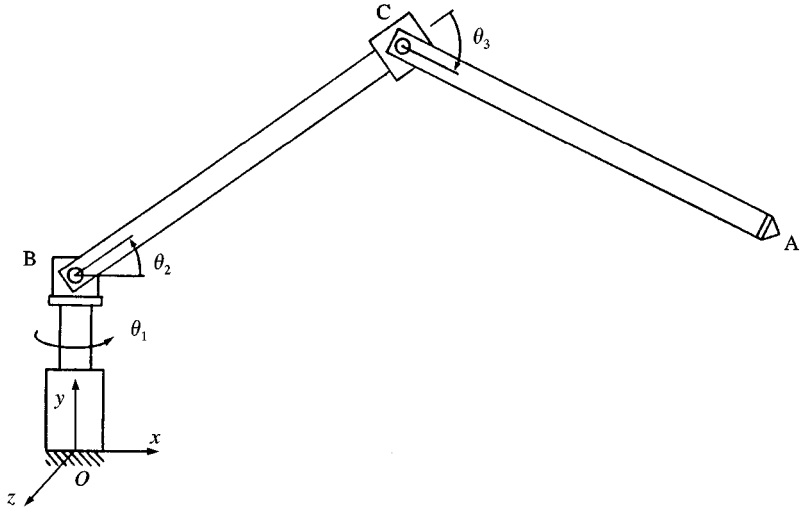

Figure 1. 3R spatial robot.

$$x_3^{\mathrm{d}} = \begin{cases} 0{\cdot}22\ \mathrm{m}, & 0 \leqslant t < T_1, \\ 0{\cdot}22 - \dfrac{0{\cdot}5}{T}\left[t - T_1 - \dfrac{T}{2\pi}\sin\dfrac{2\pi(t-T_1)}{T}\right]\mathrm{m}, & T_1 \leqslant t < T_1 + T, \\ -0{\cdot}28\ \mathrm{m}, & t \geqslant T_1 + T, \end{cases}$$

$$\lambda^{\mathrm{d}} = \begin{cases} \dfrac{50}{T_1}\left(t - \dfrac{T_1}{2\pi}\sin\dfrac{2\pi t}{T_1}\right)\mathrm{N}, & 0 \leqslant t < T_1, \\ 50\ \mathrm{N}, & T_1 \leqslant t < T_1 + T, \\ 50 - \dfrac{50}{T_2}\left[t - T_1 - T - \dfrac{T_2}{2\pi}\sin\dfrac{2\pi(t-T_1-T)}{T_2}\right]\mathrm{N}, & T_1 + T \leqslant t < T_1 + T + T_2, \\ 0, & t \geqslant T_1 + T + T_2, \end{cases}$$

where x_1, x_2, x_3 are the x, y, z co-ordinates of point A. The contact force increase period T_1, the deployment motion period T, and the contact force decrease period T_2 are $T_1 = T_2 = 0{\cdot}05$ s and $T = 0{\cdot}5$ s. Notice that there is an initial step change in the desired position. At the boundaries of the cycloidal trajectories the jerks are discontinuous.

The link dimensions are OB = 0·25 m, BC = CA = 1 m. The links are assumed to be uniform. The masses of the links are $m_1^{\mathrm{L}} = 18$ kg, $m_2^{\mathrm{L}} = 8{\cdot}6$ kg, $m_3^{\mathrm{L}} = 4{\cdot}3$ kg. The motors are assumed to be connected to the joints through harmonic drive transmission, hence are located at the joints. The motors and gear boxes have small dimensions compared to the links. The combined motor and gear box masses are $m_2^{\mathrm{M}} = 0{\cdot}4$ kg and $m_3^{\mathrm{M}} = 0{\cdot}2$ kg. The joint torsional stiffness constants are $k_1 = k_2 = k_3 = 5000$ N m/rad. Damping is neglected. The rotor moments of inertia are $I_1^{\mathrm{r}} = 4{\cdot}0 \times 10^{-5}$ kg m^2, $I_2^{\mathrm{r}} = 5{\cdot}0 \times 10^{-5}$ kg m^2, $I_3^{\mathrm{r}} = 2{\cdot}3 \times 10^{-5}$ kg m^2. The gear ratios are $r_1 = r_2 = r_3 = 100$.

In this example $n = 3$, $m = 1$ and equation (3a) becomes $g(\mathbf{x}, t) = x_1 - x_{1_0} = 0$. Hence in equation (3b) E is the first row of the manipulator Jacobian J, and G is zero. The independent co-ordinates along the constraint surface, defined in equation (5a), become $y_1 = x_2$ and $y_2 = x_3$. Hence $\mathbf{P}$ in equation (5b) is formed as $P_{1j} = J_{2j}$, $P_{2j} = J_{3j}$, $j = 1, 2, 3$, and $\mathbf{H}$ is a zero vector.

The control simulations are made by finding the control torques at each sampling time step as described in section 3. For the solution of the non-linear algebraic equation system given by equations (18) and (19), fuctional iteration is used. Equations (18) and (19) are written as

$$\dot{\boldsymbol{\theta}}_{k+1} = \begin{bmatrix} \mathbf{E}\frac{1}{h} + \dot{\mathbf{E}} \\ \mathbf{P}\frac{1}{h} + \dot{\mathbf{P}} \end{bmatrix}^{-1} \begin{bmatrix} \mathbf{E}\frac{1}{h}\dot{\boldsymbol{\theta}}_k - \dot{\mathbf{G}} \\ \mathbf{P}\frac{1}{h}\dot{\boldsymbol{\theta}}_k - \dot{\mathbf{H}} + \mathbf{z}_{k+1} \end{bmatrix}. \tag{29}$$

Starting with $\dot{\boldsymbol{\theta}}_k$ for $\dot{\boldsymbol{\theta}}_{k+1}$ in the right-hand side, equation (29) is solved for new $\dot{\boldsymbol{\theta}}_{k+1}$. Iteration continues until the norm of the difference in $\dot{\boldsymbol{\theta}}_{k+1}$ between successive

iterations is less than a small number ε. It has been observed by the numerical simulations that for $\varepsilon = 10^{-10}$, at most three iterations were sufficient.

The control torques are then applied to the actual system which can be expressed using equations (1) and (2) and the derivative of equation (3b), as

$$\begin{bmatrix} \mathbf{M} & \mathbf{0} & \mathbf{E}^{\mathrm{T}} \\ \mathbf{0} & \mathbf{I}^{\mathrm{r}} & \mathbf{0} \\ \mathbf{E} & \mathbf{0} & \mathbf{0} \end{bmatrix} \begin{bmatrix} \ddot{\boldsymbol{\theta}} \\ \ddot{\boldsymbol{\psi}} \\ \boldsymbol{\lambda} \end{bmatrix} = \begin{bmatrix} -\mathbf{Q} - \mathbf{D}(\dot{\boldsymbol{\theta}} - \dot{\boldsymbol{\psi}}) - \mathbf{K}(\boldsymbol{\theta} - \boldsymbol{\psi}) \\ \mathbf{T} - \mathbf{D}^{\mathrm{r}}\dot{\boldsymbol{\psi}} + \mathbf{D}(\dot{\boldsymbol{\theta}} - \dot{\boldsymbol{\psi}}) + \mathbf{K}(\boldsymbol{\theta} - \boldsymbol{\psi}) \\ -\dot{\mathbf{E}}\dot{\boldsymbol{\theta}} - \dot{\mathbf{G}} \end{bmatrix}. \tag{30}$$

$\ddot{\boldsymbol{\theta}}$, $\ddot{\boldsymbol{\psi}}$ and $\boldsymbol{\lambda}$ are solved from equation (30) and $\ddot{\boldsymbol{\theta}}$ and $\ddot{\boldsymbol{\psi}}$ are numerically integrated using a predictor-corrector algorithm to yield the joint and rotor position and velocity responses.

First, it is assumed that there is no modelling error and the control system is simulated without the integral terms in the command jerk rates and the command contact force second derivatives, i.e., $\mathbf{C}_5 = \mathbf{0}$, $B_3 = 0$. ITAE performance criteria are used, where $C_{1i} = 2{\cdot}1\alpha_i$, $C_{2i} = 3{\cdot}4\alpha_i^2$, $C_{3i} = 2{\cdot}7\alpha_i^3$, $C_{4i} = \alpha_i^4$, $i = 1, 2$; $B_1 = 1.4\beta$, $B_2 = \beta^2$. In the simulations $\alpha_i = 50$ rad/s, $i = 1, 2$; $\beta = 600$ rad/s, Figures 2 and 3

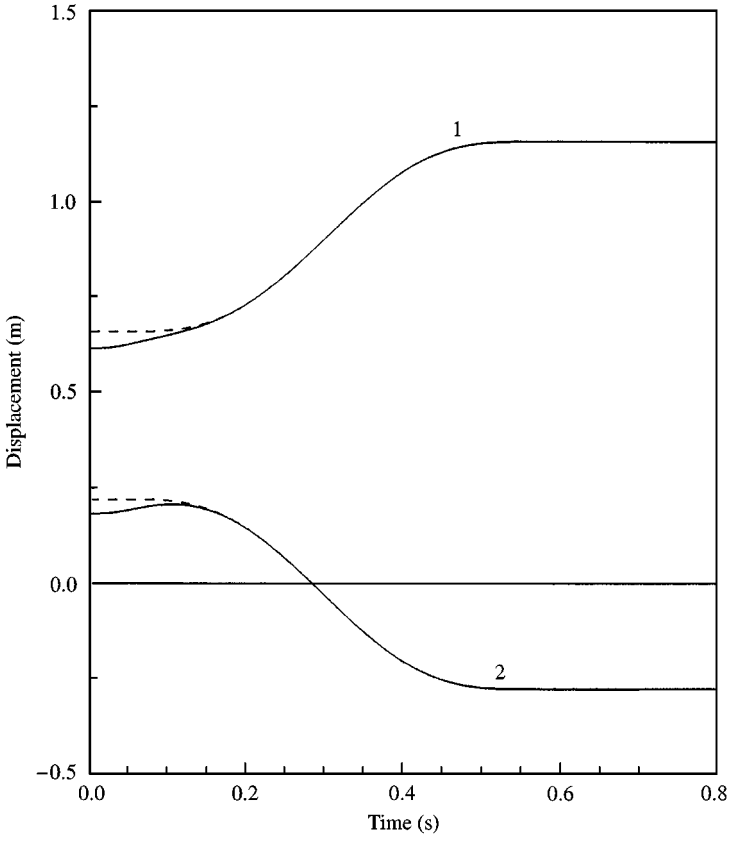

Figure 2. Position response without integral control: 1. y_1, 2. y_2, —— Response; - - - Desired.

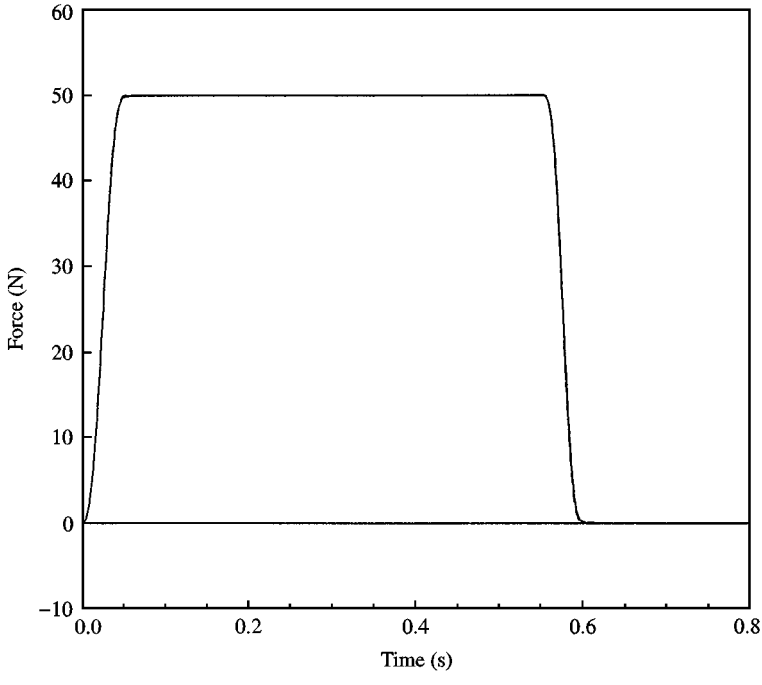

Figure 3. Contact force response without integral control: λ. —— Response; - - - Desired.

show that good tracking properties are achieved in both the motion and contact force.

To see the effects of modelling error, the robot inertia parameters and the torsional spring constants are assumed to be 20% larger in the model. When the control simulations are made using the above feedback gains, the position and contact force responses are obtained as shown in Figures 4 and 5, respectively. The tracking and steady-state errors are considerably large. The control torques are depicted in Figure 6. The errors can be reduced by increasing α_i and β. However, this produces larger control torques and necessitates smaller sampling times.

Then the integral terms in the control law are also included for improving robustness to modelling error. ITAE criteria, i.e., $C_{1i} = 2{\cdot}8\alpha_i$, $C_{2i} = 5{\cdot}0\alpha_i^2$, $C_{3i} = 5{\cdot}5\alpha_i^3$, $C_{4i} = 3{\cdot}4\alpha_i^4$, $C_{5i} = \alpha_i^5$, $i = 1, 2$; $B_1 = 1{\cdot}75\beta$, $B_2 = 2{\cdot}15\beta^2$, $B_3 = \beta^3$, and the same α_i and β are used. Figures 7 and 8 show the position and contact force responses. The tracking and steady-state errors are reduced to negligible levels. The control torques are plotted in Figure 9. The final spring deflections ($\theta_i - \psi_i$) are 0, $0{\cdot}36^\circ$ and $-0{\cdot}51^\circ$ respectively.

In the simulations a sampling time interval of 0·001 s is used (sampling freq. = 6284 rad/s). As long as the sampling frequency is chosen to be not less than about ten times the largest of the closed-loop natural frequencies, the algorithm is not sensitive to the size of the time step. The controller bandwidth can be increased if a higher sampling frequency is used.

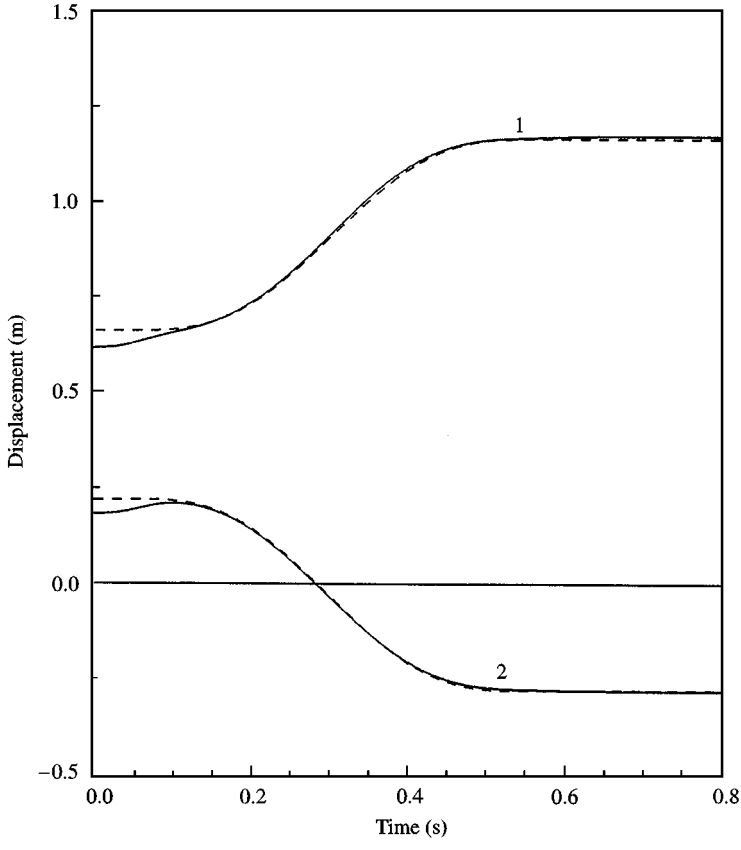

Figure 4. Position response without integral control (model error): 1. y_1, 2. y_2, — Response; - - - Desired.

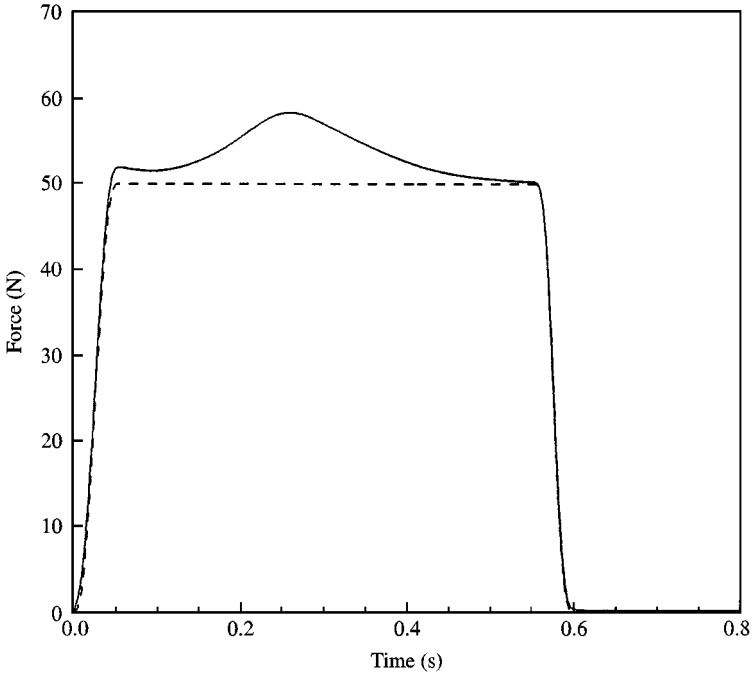

Figure 5. Contact force response without integral control (model error): λ. — Response; - - - Desired.

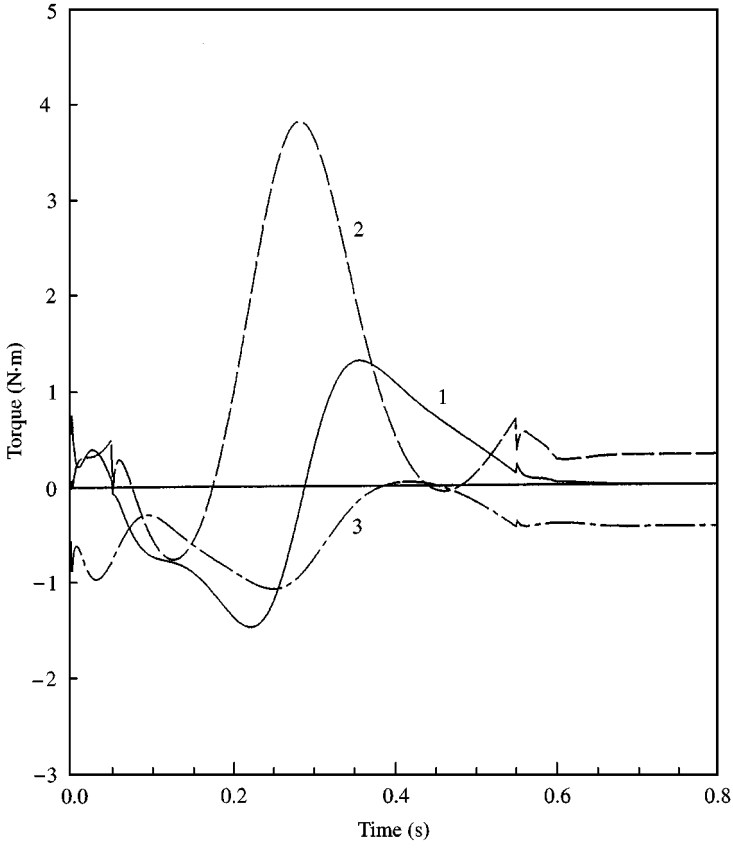

Figure 6. Control torques without integral control (model error): 1. T_1, 2. T_2, 3. T_3.

5. CONCLUSIONS

This paper has presented a hybrid force and motion trajectory tracking control law for flexible-joint robots based on solving the acceleration level inverse dynamic equations which are singular. The implicit numerical integration procedure accounts for the higher order derivative information. By the proposed method further differentiations of the equations of motion and the constraint and task equations are avoided. Since inconsistent initial values at a sampling time cause the control torques to be incorrect, the relations that the initial values should satisfy are taken into consideration. When the rotor positions are chosen to achieve the consistency, the required measurements are the joint positions, joint velocities and rotor velocities. Since the constraint surface equation is given, the contact forces are found by appropriate calculations.

One of the critical points in the algorithm is that since the control forces cannot make an instantaneous effect on the end-effector contact forces, contact force rates, end-effector accelerations and end-effector jerks, step changes in $\mathbf{\Gamma}$, $\dot{\mathbf{\Gamma}}$, $\mathbf{z}$ and $\dot{\mathbf{z}}$, require infinitely large control torques. For obtaining continuous $\mathbf{\Gamma}$, $\dot{\mathbf{\Gamma}}$, $\mathbf{z}$ and $\dot{\mathbf{z}}$ they

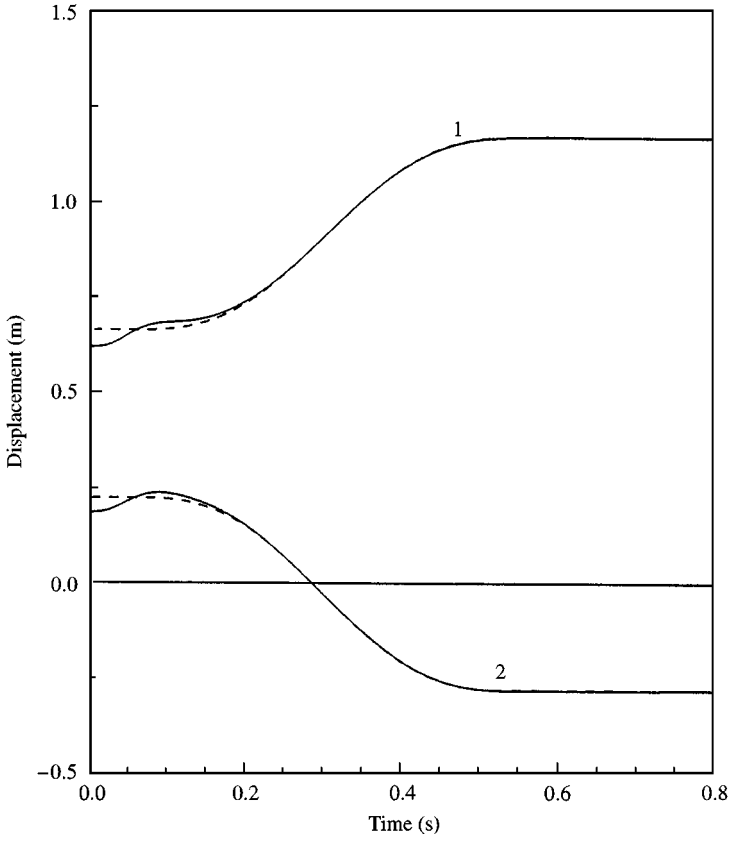

Figure 7. Position response (model error): 1. y_1, 2. y_2, — Response; - - - Desired.

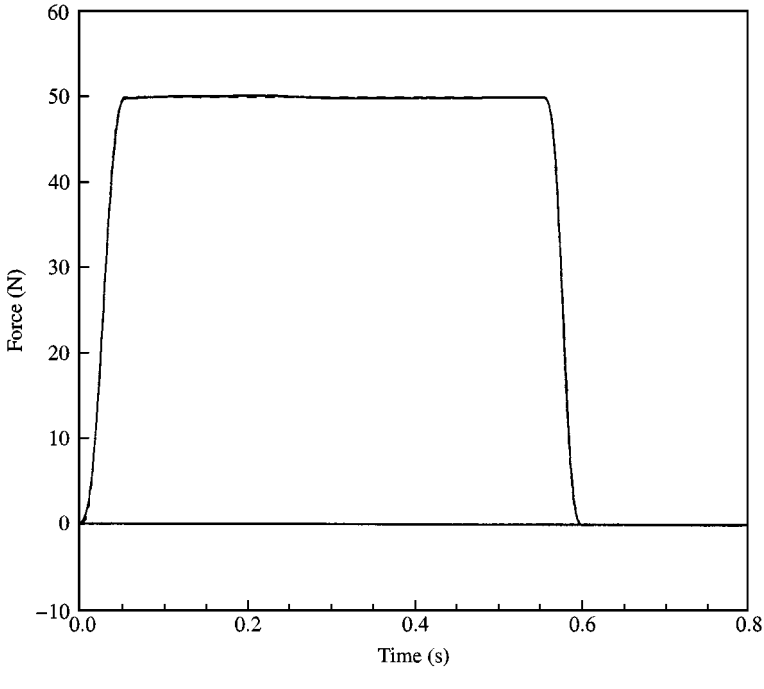

Figure 8. Contact force response (model error), λ. — Response; - - - Desired.

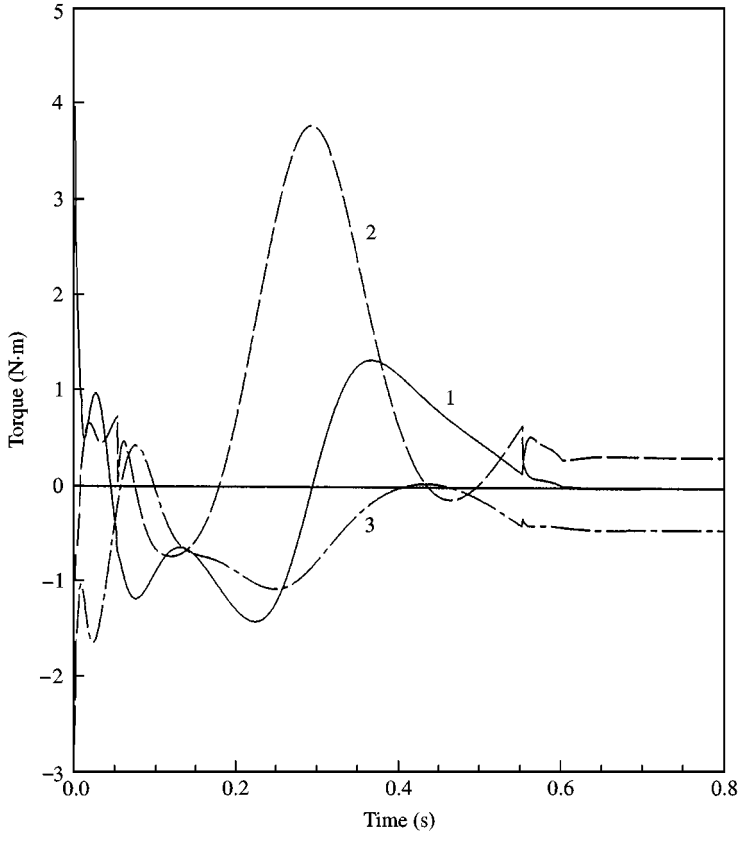

Figure 9. Control torques (model error): 1. T_1, 2. T_2, 3. T_3.

are matched at the discontinuities of the reference trajectories by freely selecting the integration constants accordingly. Hence, initial and intermediate jumps in all states of the desired force and motion trajectories are allowed.

REFERENCES

1. E. I. Rivin 1985 *Proceedings of American Control Conference, Boston, MA*, 381–382. Effective rigidity of robot structure: analysis and enhancement.
2. S. D. Eppinger and W. P. Seering 1989 *Proceedings of the IEEE Conference on Robotics and Automation*, Scottsdale, *AZ*, 392–397. Three dynamic problems in robot force control.
3. M. W. Spong 1987 *ASME Journal of Dynamic Systems Measurement and Control* **109**, 310-319. Modelling and control of elastic joint robots.
4. M. G. Forrest-Barlach and S. M. Babcock 1987 *IEEE Journal of Robotics and Automation* **3**, 75–83. Inverse dynamics task control of a complaint manipulator.
5. A. De Luca 1988 *Proceedings of the IEEE Conference on Robotics and Automation, Philadelphia*, 152–158. Dynamic control of robots with joint elasticity.
6. K. P. Jankowski and H. Van Brussel 1992 *IEEE Transactions on Robotics and Automation* **8**, 651–658. An approach to discrete inverse dynamics control of flexible-joint robots.

7. M. W. Spong 1987 *IEEE Journal of Robotics and Automation* **3**, 291–300. An integral manifold approach to the feedback control of flexible joint robots.
8. S. Gogate and Y. Lin 1993 *Robotica* **11**, 273–282. Formulation and control of robots with link and joint flexibility.
9. K. Khorasani 1992 *IEEE Transactions on Robotics and Automation* **8**, 250–267. Adaptive control of flexible-joint robots.
10. J. Lian, J. Jean and L. C. Fu 1991 *IEEE Transactions on Robotics and Automation* **7**, 540–545. Adaptive force control of single-link mechanism.
11. K. P. Jankowski and H. A. Elmaraghy 1994 *Robotica* **12**, 227–241. Inverse dynamics and feedforward controllers for high precision position/force tracking of flexible joint robots.
12. Y. R. Hu and A. A. Goldenberg 1994. *ASME Journal of Dynamic Systems, Measurement and Control* **116**, 326–335. An approach to motion and force control of coordinated robot arms in the presence of joint flexibility.
13. S. K. Ider 1995 *Journal of Robotic Systems* **12**, 569–579. Inverse dynamics of redundant manipulators using a minimum number of control forces.
14. C. W. Gear and L. R. Petzold 1984 *SIAM Journal of Numerical Analysis* **21**, 716–728. ODE methods for the solution of differential/algebraic systems.